Applied Surface Science 314 (2014) 215–220

Contents lists available at ScienceDirect

Applied Surface Science

journal homepage: www.elsevier.com/locate/apsusc

High precision patterning of ITO using femtosecond laser annealing process

Chung-Wei Cheng [a,*], Cen-Ying Lin [b]

[a] Department of Mechanical Engineering, National Chiao Tung University, No. 1001, Ta Hsueh Road, Hsinchu 30010, Taiwan
[b] ITRI Southern Region Campus, Industrial Technology Research Institute, Liujia District, Tainan City 734, Taiwan

ARTICLE INFO

Article history:
Received 1 April 2014
Received in revised form 28 May 2014
Accepted 29 June 2014
Available online 5 July 2014

Keywords:
Patterning
ITO
Femtosecond laser
Annealing
Crystallization

ABSTRACT

High precision patterning of crystalline indium tin oxide (c-ITO) patterns on amorphous ITO (a-ITO) thin films by femtosecond laser-induced crystallization with a Gaussian beam profile followed by chemical etching is demonstrated. In the proposed approach, the a-ITO thin film is selectively transformed into a c-ITO structure via a low heat affect zone and the well-defined thresholds (ablation and crystallization) supplied by the femtosecond laser pulse. The experimental results show that by careful control of the laser fluence above the crystallization threshold, c-ITO patterns with controllable line widths and ridge-free characteristics can be accomplished. By careful control of the laser fluence above the ablation threshold, fast fabrication of the two parallel sub-micro c-ITO line patterns using a single femtosecond laser beam and single scanning path can be achieved. Along-length sub-micro c-ITO line pattern is fabricated, and the feasibility of fabricating c-ITO patterns is confirmed, which are expected to be used in micro-electronics devices.

1. Introduction

Indium tin oxide (ITO) is widely used as a transparent conducting oxide (TCO) material with high transparency in the visible region of the spectrum. The resistivity of an ITO pattern should be maintained as low as possible in order to obtain a high response for functional devices, such as a liquid crystal display. Since the crystalline structure usually has a lower resistivity than an amorphous structure does, the as-deposited amorphous-ITO (a-ITO) thin film usually undergoes furnace annealing at a temperature higher than 200 °C [1] and changes to crystalline-ITO (c-ITO) film. To achieve rapid thermal heating, the laser annealing process with a nanosecond pulsed laser [2–4] or ultra-short pulsed laser [5,6] of TCO is presented. The annealed c-ITO film is then patterned by photolithography or micro-contact printing process [7]. These are complicated and time-consuming processes, e.g. the photolithographic process that involves photoresist coating and baking, photoresist exposure and developing, etching and photoresist stripping.

Laser processing is a natural technology intended for use in patterning ITO film, i.e. selectively removing the ITO and leaving the desired ITO pattern. Many researchers have investigated the ablation process irradiating from the ITO side with nanosecond [8–11], picosecond [12,13] and femtosecond lasers [14–17]. However, the ablation process requires sufficient laser energy density to evaporate the materials. Elevated ridges of the edges and ITO residue on an ablated bottom easily occur, which may cause shorting of the structure or the adjacent electrodes. To overcome the above disadvantages, Krause et al. [16] used a femtosecond laser to remove the ITO irradiating through the glass side and create almost rectangular cross-sectional groove profiles despite the Gaussian laser beam.

Since a-ITO thin film has a more rapid etching rate than the c-ITO structure [18], some researchers utilized the nanosecond pulsed laser annealing process followed by wet etching to fabricate a c-ITO pattern from a-ITO thin films [3,19–21]. Recently, researchers [22,23] have been using a high repetition rate femtosecond laser resonator (85 MHz, 12 fs) with a high numerical aperture (NA 1.3) to anneal the polycrystalline ITO film into a different phase which is more resistive in hydrochloric acid and follow up with wet etching to fabricate sub-wavelength nanostructuring. In our previous studies, a process to fabricate sub-micro c-ITO grating from a-ITO thin film based on the laser-induced periodic surface structure (LIPSS) combined with femtosecond laser-induced crystallization was presented [24]. The nanogratings were found to have a period of approximately 200 nm (i.e. one-quarter of the irradiation wavelength 800 nm). Furthermore, a crackless c-ITO pattern fabricated by the high repetition rate (80 MHz) femtosecond laser-induced

* Corresponding author. Tel.: +886 3 5712121 ext. 55126; fax: +886 3 5720634.
E-mail address: weicheng@nctu.edu.tw (C.-W. Cheng).

http://dx.doi.org/10.1016/j.apsusc.2014.06.174
0169-4332/

crystallization process with heat accumulation effect was reported [5]. However, due to the extended width caused by the heat accumulation effect, the line width of the fabricated c-ITO pattern was usually greater than that of the focused beam diameter.

In this study, a sub-micro c-ITO pattern was fabricated from a-ITO thin film based on femtosecond laser-induced crystallization with a Gaussian beam profile and followed by chemical etching. The results show that the threshold fluences (ablation and crystallization) of a-ITO thin film were well-defined, and the heat affect zone was made much smaller by careful control of the laser fluence accomplishing c-ITO patterns with controllable line width and ridge-free characteristics. Furthermore, fast fabrication of the two parallel sub-micro c-ITO line patterns using a single femtosecond laser beam and single scanning path can be achieved. Finally, a long-length sub-micro c-ITO line patterns is fabricated, and the feasibility of fabricating c-ITO patterns from a-ITO thin film is confirmed.

2. Experimental setup

Amorphous ITO thin films, with a thickness of approximately 100 nm, were deposited on glass substrates (NEG OA10) using a DC magnetron sputtering system using the In_2O_3 (90 wt%):SnO_2 (10 wt%) target. The thin films were then irradiated using a regenerative amplified mode-locked Ti:Sapphire laser (SPIT FIRE, Spectra-Physics) with a central wavelength of 800 nm, a repetition rate of 1 kHz and a pulse duration of ~120 fs. The laser beam was linearly polarized and spatially filtered, resulting in an essentially Gaussian profile. To adjust the energy of the laser beam, the linear polarized Gaussian laser beam was attenuated by a rotatable half-wave plate and a polarizing beam splitter. To measure the laser energy, a certain fraction of the laser beam was split off by a beam splitter and measured with a power detector (818P-001-12, Newport). The powers of the reflected and transmitted laser beams to different angle of half-wave plate were measured with power detectors, and a calibration table between reflected and transmitted components was obtained. The transmitted component was passed through a mechanical shutter and reflective mirror system such that it entered an objective lens (numerical aperture 0.26, M Plan Apo NIR, Mitutoyo) and was subsequently incident in the normal direction on the surface of an a-ITO coated specimen mounted on an *X*–*Y* positioning stage. The theoretical focal spot diameter was calculated to be approximately 3.75 μm (1.22λ/NA, λ = 800 nm is the wavelength, NA = 0.26 is the numerical aperture). The ITO patterns were then fabricated by translating the sample stage under the control of a PC-based micro-positioning system with a precision of better than 1 μm.

After femtosecond laser processing, the specimens were immersed in 0.05 mol/L oxalic acid etchant at 50 °C for 2.5 min. Due to the more rapid etching rate of the a-ITO thin film than the c-ITO structure [18], the etching process resulted in the complete removal of the non-irradiated a-ITO film, leaving only the crystalline c-ITO pattern.

The surface characteristics of the structures were observed using scanning electron microscopy (SEM, FE-SEM 7001). Cross-sectional samples perpendicular to the c-ITO line patterns were prepared using a focused ion beam system (FIB, SMI 3050) and were observed via transmission electron microscopy (TEM, FEI Tecnai G2 20 S-Twin). The FIB, with a gallium ion source, was used to mill the c-ITO down to a thickness of 100–200 nm in order to make a cross-section sample.

3. Results and discussion

Fig. 1 shows the tile-view SEM images of the c-ITO structures (a section of a line pattern) formed at laser powers: 30, 20, 19 μW (30, 20, 19 nJ) and a scanning speed of 0.05 mm/s with linearly polarized light orientated in the perpendicular direction to the scanning path, respectively. It can be seen that the un-irradiated a-ITO area was removed by an etching solution to form a c-ITO structure on the glass substrate. The c-ITO line widths were measured to be 2.0, 1.1 and 0.8 μm, respectively. Note that the modified region, before wet etching, appears as a contrast, and no material was removed from the surface (not shown), and the experiment results in this study are all shown in an etched condition. In Fig. 1(a), few nanostructures were found at the center of the line pattern; this was caused because the irradiated laser fluence is near the ablation threshold of the ITO film, and a laser-induced periodic surface structure occurred. A more detailed discussion can be found in an earlier study [24]. Since the laser fluences of Fig. 1(b) and (c) were below the ablation threshold, no nanostructures were found at the line pattern.

Fig. 2 shows the top-view of SEM images of c-ITO structures formed at laser powers of 90, 70 and 50 μW (90, 70, 50 nJ) and at a scanning speed of 0.05 mm/s with linearly polarized light orientated in a perpendicular direction to the scanning path, respectively. The ablation line widths were measured to be 2.6, 2.1 and 1.4 μm, respectively. Since the peak intensity of the laser beam is higher than the ablation threshold of the ITO film, the center area is directly ablated. The irradiation intensity of the laser beam has a Gaussian distribution, the outer edges of the irradiated paths are subject to a lower energy input, and thus, it can be seen that the ablated channels are bordered on either side of the sub-micro ~0.5 μm c-ITO line pattern, which is smaller than the theoretical focal spot diameter 3.75 μm (see Section 2). The nanostructures adjacent to the c-ITO line pattern were also caused because the irradiated laser fluence at this area is near the ablation threshold of the ITO film, and a laser-induced periodic surface structure occurred.

The c-ITO structures are further investigated using an X-ray energy dispersive spectrometer (EDS). Fig. 3 shows the point-focused EDS at the micro c-ITO line pattern of Fig. 1(a) and sub-micro c-ITO line pattern of Fig. 2(a), respectively. The EDS profile presents the main compositions of ITO as In, Sn and O. The c-ITO pattern composition remains unchanged by the femtosecond laser annealing and wet etching process.

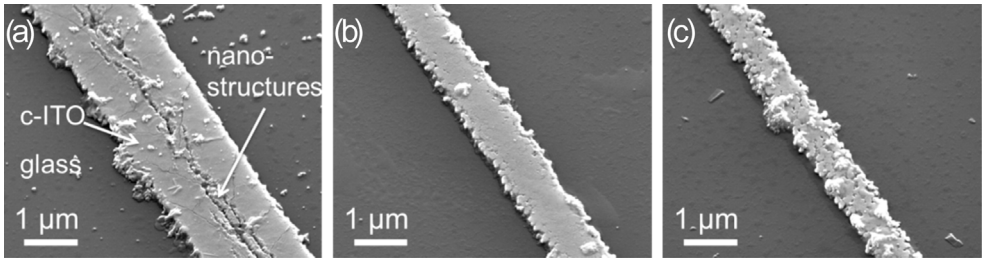

Fig. 1. SEM images of c-ITO line patterns fabricated under laser powers of: (a) 30 μW, (b) 20 μW, (c) 19 μW. The scanning speed was 0.05 mm/s in all cases.

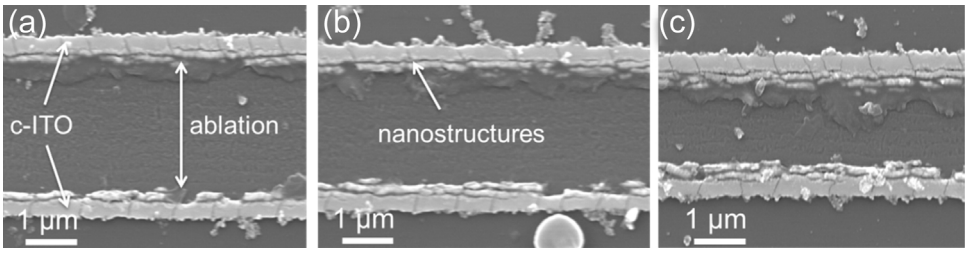

Fig. 2. SEM images of c-ITO structures fabricated under laser powers of: (a) 90 μW, (b) 70 μW, (c) 50 μW. The scanning speed was 0.05 mm/s in all cases.

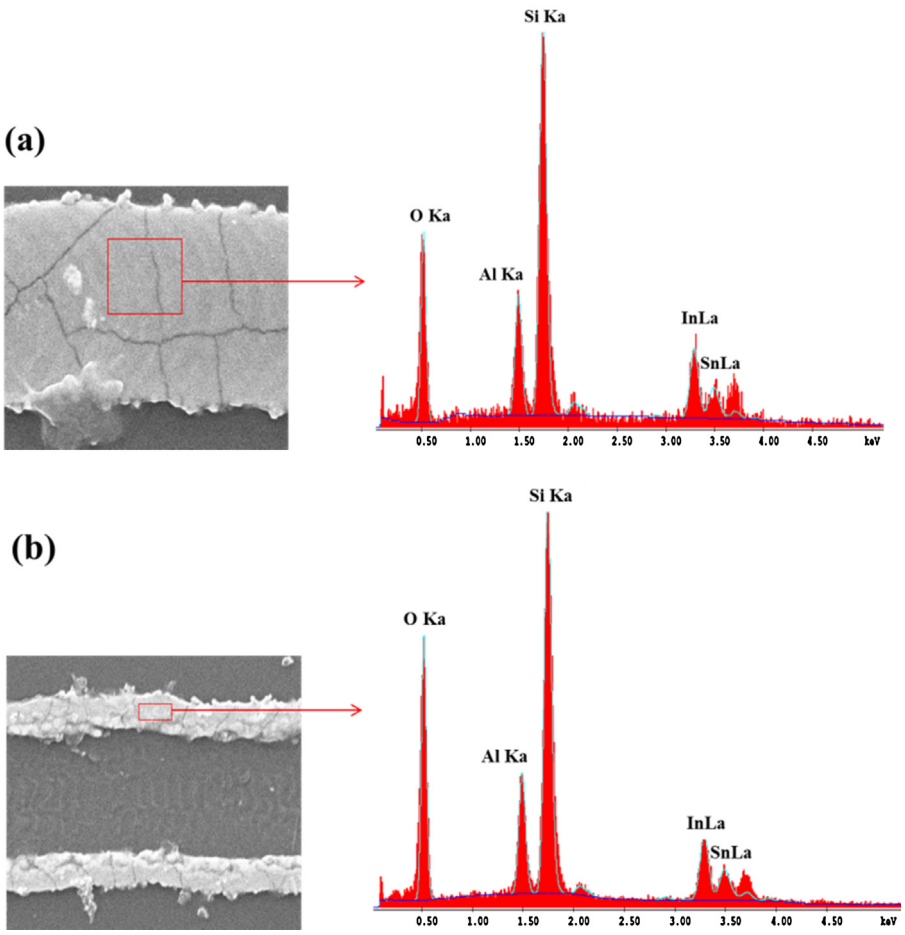

Fig. 3. Point-focused EDS resultsfor (a) c-ITO line pattern of Fig. 1(a); and (b) sub-micro c-ITO line pattern of Fig. 2(a).

In Figs. 1 and 2, we see that the crystallization and ablation widths all decrease with decreasing laser power and seem to be sensitive to the spatial intensity distribution of the focused laser beam. Assuming a Gaussian laser beam profile, the laser focus spot size at the sample surface can be determined by plotting the square of the line width against the laser energy using alogarithmic scale [25].

Fig. 4 illustrates the variation of square of the line widths with laser energy. The straight lines curve-fitted (correlation coefficient $R^2 \sim 0.99$) from the experimental data confirm the logarithmic dependence between the square of line width and the laser energy. The slopes of the fitted lines are found to be 7.3067 and 8.2384, respectively. Accordingly, the laser beam focused radii are approximated to be $\sqrt{(7.3067/2)} = 1.91\,\mu m$ and $\sqrt{(8.2384/2)} = 2.03\,\mu m$, respectively, which are all close to the theoretical focus spot radius at 1.875 μm. Then, the threshold energy for crystallization and ablation can be computed to be 17.3 nJ and 40.1 nJ, respectively. The threshold fluence for crystallization and ablation was further computed to be 0.15 J/cm^2 and 0.31 J/cm^2, respectively. The estimated ablation threshold fluence 0.31 J/cm^2 is a little higher than the value

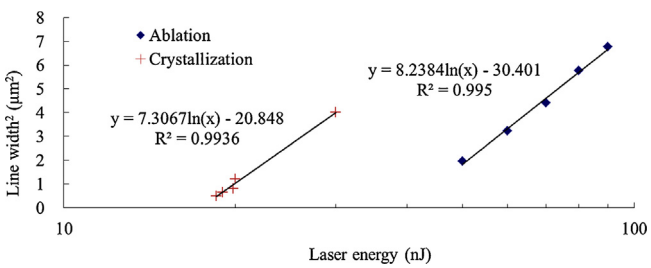

Fig. 4. Variation in the square of the ablation line width and crystallization line width with laser energy.

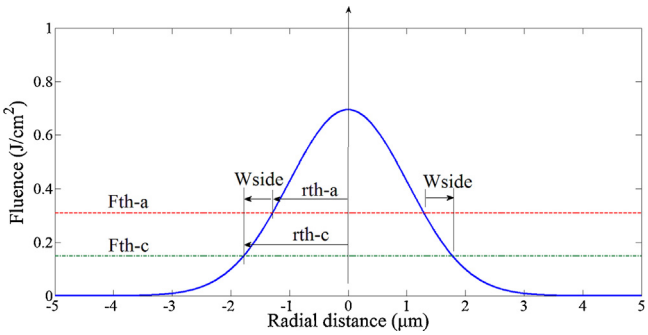

Fig. 5. The energy density distribution with respect to the radial distance.

0.21 J/cm^2 using femtosecond laser systems (800 nm, 1 kHz) with shorter pulse duration (60 fs) previously reported [17].

Due to the features of short pulse duration time and extremely high peak power, femtosecond laser pulse has a very high electromagnetic field intensity at its focus. The electrons are bound to absorb multi-photons to directly transit from the binding energy level to the free energy level. Hence, the femtosecond laser can realize the micro-marching inside transparent glass material without extremely low thermal effects, and the processing zone can be smaller than the focus size [26]. In this study, since the band gap in a-ITO thin film (~3.6 eV) is much larger than the photon energy (800 nm, 1.55 eV), the incident focused laser with high peak power intensity (~2.6×10^{12} W/cm^2 for laser fluence 0.31 J/cm^2 of 120 fs) creates a dense electron plasma through multi-photon excitation [27] at the irradiated material. It can precisely confine the absorption regions, thereby determining the crystallization threshold of the a-ITO. Accordingly, operating the peak fluence at the levels below the ablation threshold and higher than the crystallization threshold allows for selective fast thermal processing with a low heat-affected zone. c-ITO line widths less than the laser beam focus diameter can be achieved (see Fig. 1).

Since the irradiation intensity of the laser beam has a Gaussian distribution, the distribution of energy density (fluence) across the laser beam can be given by:

$$F(r) = F_p e^{-2r^2/\omega^2} \tag{1}$$

where F_p is the peak fluence at the beam center, r is the radial coordinate of distance from the beam propagation axis and ω is the beam radius (at e^{-2}).

Fig. 5 shows an example of energy density distribution in respect to the radial distance, where $F_p = 0.7$ J/cm^2 (laser power 90 μW) and $\omega = 2.03$ μm. The F_{th_a} and F_{th_c} are the threshold fluences for ablation and crystallization of ITO, i.e. 0.31 and 0.15 J/cm^2, respectively. Crystallization takes place in areas where the laser fluence exceeds the crystallization threshold F_{th_c} but is less than the ablation threshold F_{th_a}, resulting in the crystallization width (W_{side}). The fluence at the radial distances, r_{th_a} and r_{th_c}, are consistent with the Gaussian beam profile defined in Eq. (1):

$$F_{th\_a} = F(r_{th\_a}) = F_p e^{-2(r_{th\_a}^2/\omega^2)} \tag{2}$$

$$F_{th\_c} = F(r_{th\_c}) = F_p e^{-2(r_{th\_c}^2/\omega^2)} \tag{3}$$

The r_{th_a} and r_{th_c}, on the peak fluence F_p could be expressed as:

$$r_{th\_a}^2 = \frac{\omega^2}{2} \ln \frac{F_p}{F_{th\_a}} \tag{4}$$

$$r_{th\_c}^2 = \frac{\omega^2}{2} \ln \frac{F_p}{F_{th\_c}} \tag{5}$$

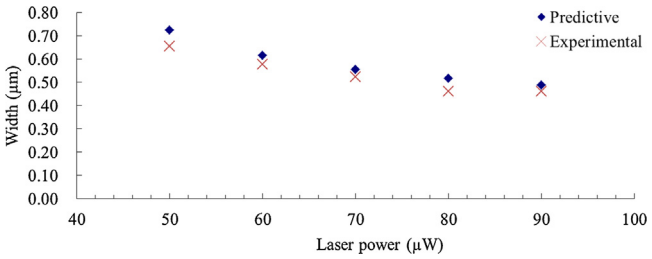

Fig. 6. Predictive and experimental crystallization widths W_{side}

From Eqs. (4) and (5), the crystallization width W_{side} on the peak fluence F_p can then be expressed as:

$$W_{side} = r_{th\_c} - r_{th\_a} \tag{6}$$

$$= \frac{\omega}{\sqrt{2}} \left(\left[\ln \frac{F_p}{F_{th\_c}} \right]^{1/2} - \left[\ln \frac{F_p}{F_{th\_a}} \right]^{1/2} \right)$$

Then the overlapping ratio at the crystallization width W_{side} can be calculated as

$$o_{W_{side}} = 1 - \frac{s}{2\omega f} \tag{7}$$

where s is the scanning speed, f is the laser repetition rate.

Equation (6) was used to calculate predictive crystallization width W_{side} and compare it to experimental results. Fig. 6 shows the predictive and experimental crystallization widths irradiated by laser power 50–90 μW. The experimental widths are in agreement with predictions. The average difference between the predictive and experimental results is 0.0434 μm caused by the energy stability of the femtosecond laser during irradiation, measurement error of the laser beam radius, and nonlinear optics effects. For example, when the energy stability of the femtosecond laser source is ±1%, given the laser power 50 μW, the maximum deviation of the crystallization width W_{side} is computed to be 0.02 μm. When the measurement error of the laser beam radius is ±1%, e.g. the $\omega = 2.03$ μm is reduced to 1.99 μm, given the laser power of 50 μW, the maximum deviation of the crystallization width W_{side} is computed to be 0.04 μm.

From Fig. 5, the track separation width between the two parallel sub-micro c-ITO line patterns ($2 \times r_{th\_a}$) can be calculated from Eq. (4). Fig. 7 shows the predictive and experimental track separation widths irradiated by laser power 50–90 μW. The experimental widths are in agreement with predictions, and the maximum deviation is computed to be 0.04 μm.

Fig. 8(a) presents a cross-sectional TEM image of the line pattern shown in Fig. 1(a). Note, that this image was captured from the line edge to near the center, and the platinum layer is a protective layer deposited on the c-ITO structure prior to FIB micromachining. The thickness of the c-ITO structure is found to be the same as that of the as-deposited a-ITO thin film, i.e. ~100 nm. This means that the irradiated laser energy is sufficient to crystallize a-ITO thin

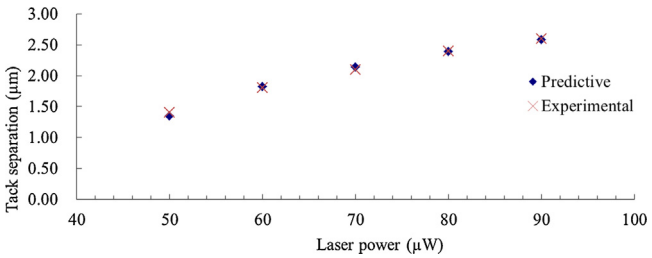

Fig. 7. Predictive and experimental track separation between the two parallel sub-micro c-ITO line patterns.

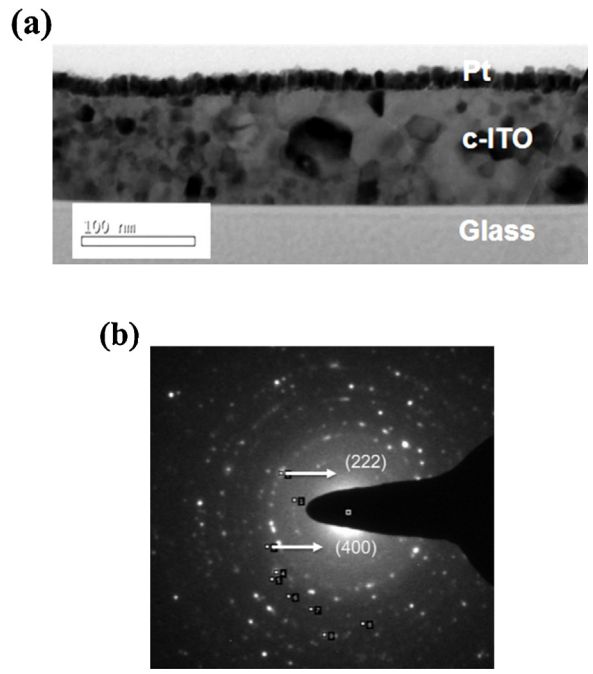

Fig. 8. (a) Cross-sectional TEM image of the line pattern shown in Fig. 1(a), and (b) electron diffraction pattern.

film. Since the irradiation intensity of the laser beam has a Gaussian distribution, the average diameter of grains within the c-ITO pattern is found to have a small value at the edge and a large one near the center. The electron diffraction pattern, shown in Fig. 8(b), indicates that the ITO pattern is crystalline with strong (2 2 2) and (4 0 0) orientations.

To demonstrate the long-length fabrication capability, Fig. 9 shows the SEM image of the sub-micro c-ITO line patterns using a single femtosecond laser beam and a single scanning path with a laser power of 90 μW at scanning speeds of 0.05 mm/s, 0.25 mm/s and 0.5 mm/s, respectively. For every single scanning path, two uniform and parallel sub-micro c-ITO line patterns can be fabricated.

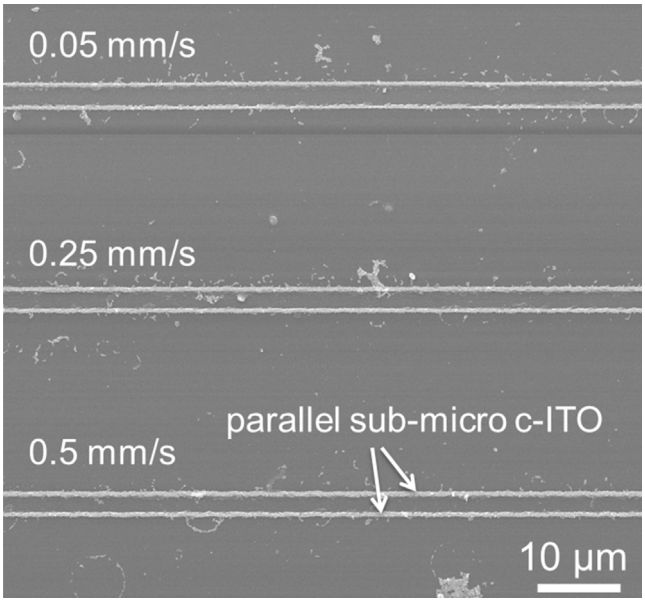

Fig. 9. SEM images of the parallel sub-micro c-ITO line patterns fabricated using a single scanning path with a laser power of 90 μW at scanning speeds of 0.05 mm/s, 0.25 mm/s and 0.5 mm/s, respectively.

The maximum scanning speed in this experiment is limited to the low laser repetition rate (i.e. 1 kHz). From Eq. (7), the overlapping ratio at the crystallization width is calculated to be ~88% for scanning speed of $s = 0.5$ mm, the $\omega = 2.03$ μm, and $f = 1$ kHz. Note that to enhance the line edge quality, the overlapping ratio larger than 80% is required for the Gaussian distribution. The scanning speed can be further increased by the high repetition rate femtosecond laser, e.g. 100 kHz.

4. Conclusions

This study reports a fabrication process of c-ITO patterns using femtosecond laser-induced crystallization with a Gaussian beam profile followed by chemical etching. The experimental results have demonstrated that the ablation and crystallization threshold fluences of a-ITO thin film are well-defined, the line width of the c-ITO patterns is controllable and the c-ITO line is completely crystallized throughout the film. It was found that the Gaussian beam profile significantly improved the patterning accuracy and fast fabrication of the two parallel sub-micro (~0.5 μm) c-ITO line patterns using a single femtosecond laser beam and a single scanning path can be achieved. A long-length sub-micro c-ITO line patterns is fabricated, and the proposed patterning technique is confirmed to provide a highly precise means of fabricating c-ITO structures required in a wide range of micro-electronic devices.

Acknowledgments

We thank Wei-Chin Shen and Yi-Ju Lee for their help withthe experiments and Jenq-Shyong Chen for useful discussion.

References

[1] H. Morikawa, M. Fujita, Crystallization and electrical property change on the annealing of amorphous indium-oxide and indium-tin-oxide thin films, Thin Solid Films 359 (2000) 61–67.
[2] W. Chung, M.O. Thompson, P. Wickboldt, D. Toet, P.G. Carey, Room temperature indium tin oxide by XeCl excimer laser annealing for flexible display, Thin Solid Films 460 (2004) 291–294.
[3] G. Legeay, X. Castel, R. Benzerga, J. Pinel, Excimer laser beam/ITO interaction: from laser processing to surface reaction, Phys. Status Solidi 5 (2008) 3248–3254.
[4] S.-F. Tseng, W.-T. Hsiao, D. Chiang, K.-C. Huang, C.-P. Chou, Mechanical and optoelectric properties of post-annealed fluorine-doped tin oxide films by ultraviolet laser irradiation, Appl. Surf. Sci. 257 (2011) 7204–7209.
[5] C.-W. Cheng, C.-Y. Lin, W.-C. Shen, Y.-J. Lee, J.-S. Chen, Patterning crystalline indium tin oxide by high repetition rate femtosecond laser-induced crystallization, Thin Solid Films 518 (2010) 7138–7142.
[6] D. Scorticati, A. Illiberi, T. Bor, S.W.H. Eijt, H. Schut, G.R.B.E. Römer, D.F. de Lange, A.J.H. Veld, Annealing of SnO2 thin films by ultra-short laser pulses, Opt. Express 22 (2014) A607–A621.
[7] T.L. Breen, P.M. Fryer, R.W. Nunes, M.E. Rothwell, Patterning indium tin oxide and indium zinc oxide using micro contact printing and wet etching, Langmuir 18 (2001) 194–197.
[8] O. Yavas, M. Takai, High-speed maskless laser patterning of indium tin oxide thin films, Appl. Phys. Lett. 73 (1998) 2558–2560.
[9] O. Yavas, M. Takai, Effect of substrate absorption on the efficiency of laser patterning of indium tin oxide thin films, J. Appl. Phys. 85 (1999) 4207–4212.
[10] M.-F. Chen, Y.-P. Chen, W.-T. Hsiao, Z.-P. Gu, Laser direct write patterning technique of indium tin oxide film, Thin Solid Films 515 (2007) 8515–8518.
[11] Z.H. Li, E.S. Cho, S.J. Kwon, A new laser direct etching method of indium tin oxide electrode for application to alternative current plasma display panel, Appl. Surf. Sci. 255 (2009) 9843–9846.
[12] G. Raciukaitis, M. Brikas, M. Gedvilas, T. Rakickas, Patterning of indium-tin oxide on glass with picosecond lasers, Appl. Surf. Sci. 253 (2007) 6570–6574.
[13] S. Xiao, E. Gurevich, A. Ostendorf, Incubation effect and its influence on laser patterning of ITO thin film, Appl. Phys. A 107 (2012) 333–338.
[14] M. Park, B.H. Chon, H.S. Kim, S.C. Jeoung, D. Kim, J.I. Lee, H.Y. Chu, H.R. Kim, Ultrafast laser ablation of indium tin oxide thin films for organic light-emitting diode application, Opt. Lasers Eng. 44 (2006) 138–146.
[15] H.W. Choi, D.F. Farson, J. Bovatsek, A. Arai, D. Ashkenasi, Direct-write patterning of indium-tin-oxide film by high pulse repetition frequency femtosecond laser ablation, Appl. Opt. 46 (2007) 5792–5799.

[16] S. Krause, P.T. Miclea, F. Steudel, S. Schweizer, G. Seifert, Precise microstructuring of indium-tin oxide thin films on glass by selective femtosecond laser ablation, EPJ Photovolt. 4 (2013) 40601.
[17] Q.M. Bian, X.M. Yu, B.Z. Zhao, Z.H. Chang, S.T. Lei, Femtosecond laser ablation of indium tin-oxide narrow grooves for thin film solar cells, Opt. Laser Technol. 45 (2013) 395–401.
[18] H. Hosono, M. Kurita, H. Kawazoe, Excimer laser crystallization of amorphous indium-tin-oxide and its application to fine patterning, Jpn. J. Appl. Phys. Lett. 37 (1998) L1119–L1121.
[19] J. Chae, L. Jang, K. Jain, High-resolution, resistless patterning of indium-tin-oxide thin films using excimer laser projection annealing process, Mater. Lett. 64 (2010) 948–950.
[20] C.-W. Cheng, J.-S. Chen, H.-H. Chen, Patterning of crystalline ITO using infrared nanosecond fiber laser pulses, Mater. Manuf. Process. 25 (2010) 684–688.
[21] C.J. Lee, H.K. Lin, C.H. Li, L.X. Chen, C.C. Lee, C.W. Wu, J.C. Huang, A study on electric properties for pulse laser annealing of ITO film after wet etching, Thin Solid Films 522 (2012) 330–335.
[22] M. Straub, M. Afshar, D. Feili, H. Seidel, K. König, Efficient nanostructure formation on silicon surfaces and in indium tin oxide thin films by sub-15 fs pulsed near-infrared laser light, Phys. Procedia B 12 (2011) 16–23.
[23] K. König, A. Uchugonova, M. Straub, H. Zhang, M. Licht, M. Afshar, D. Feili, H. Seidel, Sub-100 nm material processing and imaging with a sub-15 femtosecond laser scanning microscope, J. Laser Appl. 24 (2012) 042009.
[24] C.W. Cheng, W.C. Shen, C.Y. Lin, Y.J. Lee, J.S. Chen, Fabrication of micro/nano crystalline ITO structures by femtosecond laser pulses, Appl. Phys. A: Mater. Sci. Process. 101 (2010) 243–248.
[25] J.M. Liu, Simple technique for measurements of pulsed Gaussian-beam spot sizes, Opt. Lett. 7 (1982) 196–198.
[26] R.R. Gattass, E. Mazur, Femtosecond laser micromachining in transparent materials, Nat. Photon. 2 (2008) 219–225.
[27] M. Afshar, M. Straub, H. Voellm, D. Feili, K. Koenig, H. Seidel, Sub-100 nm structuring of indium-tin-oxide thin films by sub-15 femtosecond pulsed near-infrared laser light, Opt. Lett. 37 (2012) 563–565.